AIAA 2002-0856

Numerical Predictions and Experimental Results of Air Flow in a Smooth Quarter-Scale Nacelle

A. R. Black and J. M. Suo-Anttila
Sandia National Laboratories
Albuquerque, NM

P. J. Disimile
USAF 46 TW Aerospace Survivability and Safety Flight
Wright-Patterson Air Force Base, OH

J. R. Tucker
Applied Research Associates, Inc.
Dayton, OH

40th Aerospace Sciences Meeting and Exhibit
14-17 January 2002
Reno, Nevada

AIAA Paper 2002-0856

NUMERICAL PREDICTIONS AND EXPERIMENTAL RESULTS OF AIR FLOW IN A SMOOTH QUARTER-SCALE NACELLE

Amalia R. Black, Jill M. Suo-Anttila
Sandia National Laboratories*, Albuquerque, NM 87185

Peter J. Disimile
USAF 46 TW Aerospace Survivability and Safety Flight
Wright-Patterson Air Force Base, OH 45433

James R. Tucker
Applied Research Associates, Inc., Dayton, OH 45433

Abstract

Fires in aircraft engine nacelles must be rapidly suppressed to avoid loss of life and property. The design of new and retrofit suppression systems has become significantly more challenging due to the ban on production of Halon 1301 for environmental concerns. Since fire dynamics and the transport of suppressants within the nacelle are both largely determined by the available air flow, efforts to define systems using less effective suppressants greatly benefit from characterization of nacelle air flow fields. A combined experimental and computational study of nacelle air flow therefore has been initiated. Calculations have been performed using both CFD-ACE (a Computational Fluid Dynamics (CFD) model with a body-fitted coordinate grid) and VULCAN (a CFD-based fire field model with a Cartesian "brick" shaped grid). A quarter-scale test fixture was designed and fabricated for the purpose of obtaining spatially-resolved measurements of velocity and turbulence intensity in a smooth nacelle. Numerical calculations have been performed for the conditions of the experiment and comparisons with experimental results obtained from the quarter-scale test fixture are discussed. In addition, numerical simulations were performed to assess the sensitivity of the predictions to the grid size and to the turbulence models with and without wall functions. In general, the velocity predictions show very good agreement with the data in the center of the channel but deviate near the walls. The turbulence intensity results tend to amplify the differences in velocity, although most of the trends are in agreement. In addition, there were some differences between VULCAN and CFD-ACE results in the angled wall regions due to the Cartesian grid structure used by the VULCAN code. Also, the experimental data tended to show poorer resolution near the walls of the transition ducts. The increased uncertainty in the data highlights some of the challenges in getting data near the walls due to the low signal to noise ratio. Overall, this effort provided a benchmark case for both the VULCAN and CFD-ACE codes for the application of interest.

Introduction

Fires in aircraft engine nacelles pose a considerable risk to the safety and survivability of military and commercial aircraft. Effective systems and strategies are needed to suppress or extinguish these fires prior to the infliction of significant structural damage. The design of new and retrofit suppression systems and strategies have become considerably more challenging due to the demise of Halon 1301 production dictated by the Montreal Protocol and subsequent Copenhagen amendment. Despite extensive research, alternative suppressants with a per-unit mass chemical effectiveness equivalent to Halon 1301 as well as acceptable levels of toxicity, Global Warming Potential (GWP), and Ozone Depletion Potential (ODP) have yet to be discovered. To avoid the large weight penalties of

---

* Sandia is a multiprogram laboratory operated by Sandia Corporation, a Lockheed Martin Company, for the United States Department of Energy under Contract DE-AC04-94-AL85000.

carrying additional agent, it is useful to examine additional factors that influence suppression system performance. These factors include the characterization of the fire environment (to determine actual suppressant effectiveness requirements) and the transport of suppressant (to determine how to best ensure delivery of the suppressant to the fire). Both of these factors require knowledge of the flow field in engine nacelles.

Presently, aircraft survivability and suppression system proving tests are performed under conditions intended to replicate the nacelle air flow while the aircraft is in flight. Test fixtures, such as the Aircraft Engine Nacelle Fire Test Simulator (AENFTS) facility at the 46 Test Wing Aerospace Survivability and Safety Flight at Wright-Patterson Air Force Base (WPAFB) in Dayton Ohio, have been constructed to represent the long, slender, geometries typical of aircraft nacelles. Extensive sets of experiments (with varying degrees of complexity in the internal geometry) have been conducted to evaluate the performance of fire suppression systems and strategies. These tests and experiments have provided significant insight into the essential and salient features of successful suppressant systems, and serve as the basis for present system acceptance. However, the results from these tests, particularly when fire extinguishment (as opposed to cold flow tests) is the focus, are often difficult to understand due to the lack of a well-characterized flow field.

Due primarily to geometric complexities, efforts to characterize the flow field in engine nacelles using computational fluid dynamics (CFD) have been limited to simplified cases. Previous calculations include analysis performed by Hamins et al. [1] of agent transport for the extensive set of tests performed in the AENFTS for the Halon Alternatives Research Program for Aircraft Engine Nacelles and Dry Bays [2, 3]. These calculations were performed using the commercially-available CFX model. Marginal agreement between calculation results and experimental data was obtained. In some cases, opposite trends were observed in the calculations and experimental results. Additional calculations of a smooth F18 nacelle geometry with agent release via solid propellant gas generator were performed by Lopez et al. [4]. Results from this analysis were consistent with trends observed in data from simulator tests at the Naval Air Warfare Center at China Lake. Sufficient data were not available to rigorously validate the model predictions.

In the present work, reduced (1/4) scale experiments (to allow access of appropriate diagnostics), guided by pre-test calculations, were performed at the 46 Test Wing. Flow conditions were Reynolds number scaled to match the extensive set of experiments performed in the AENFTS [2, 3]. Calculations were performed and compared with experimental data at multiple cross sections within the flow field. During the first stage of this endeavor, pre-test calculations were performed to assist in the design and execution of the experiments. These experiments were required to gain the necessary knowledge for this class of flows. Based on the pre-test calculations, a test fixture was designed and experiments were conducted to characterize the flow in the smooth nacelle. Post-test simulations were conducted using both CFD-ACE and VULCAN for the conditions of the experiments. This paper presents the results from the post-test simulations using the geometry and boundary conditions from the experiments and compares the CFD code results with the experimental measurements.

The primary flow field calculations presented here were performed using the CFD-ACE model. The model features body-fitted coordinates, which accurately represent smooth circular geometries. Although capable of simulating reacting flows, the CFD-ACE code does not contain the models for participating media radiation heat transfer, turbulent combustion, and soot needed to simulate fires. These fire physics models are included in the VULCAN fire field model, but the VULCAN model approximates the geometry using a rectangular "brick" grid to facilitate the rapid solution of participating media radiation. Although many nacelle fire cases can be addressed without modeling the fire physics [4], it is ultimately desirable to be able to represent the heat transfer from the fire and fire suppression effects, such as the influence of turbulent flame strain combined with fuel/air mixture fraction. Both models have therefore been applied in the pre-test and post-test calculations. The flow solution yielded by the approximate mesh used in the VULCAN code is compared with the results provided by the CFD-ACE modeling to quantify the effect of the more rudimentary VULCAN mesh. In an attempt to validate the CFD codes, results from both codes are compared to experimental results. Additional simulations were also performed to assess the sensitivity of the predictions to the grid size and to the turbulence models with and without wall functions.

Experimental Details

Quarter-Scale Flow Facility

The quarter-scale flow facility (Figure 1) is located in Range A of the Aircraft Survivability Research Facility at WPAFB. The facility consists of an external blower, a flow conditioning section, a quarter-scale nacelle test section, and optical measurement diagnostics. Ambient air is supplied to the facility using an external blower. The air is drawn into the blower

inlet and directed to the quarter-scale nacelle simulator through a combination of 152.4 mm (6 in ID) PVC plastic and acrylic tubing. To prevent blower vibrations from being transferred to the simulator, a flexible rubber expansion joint was placed between the blower exit and the PVC air supply tube. At the exit of the supply tube, the flow enters a conditioning section consisting of stainless-steel tubes and fine mesh stainless steel screens to minimize flow disturbances introduced by the blower. After exiting the conditioning section, the air stream travels an additional 45 diameters to the nacelle inlet transition duct (ITD).

At the entrance to the ITD, the flow undergoes a change from pipe flow to diverging annular flow. This change in flow field geometry is accomplished using a machined Teflon cone, with a sharp leading edge, centered within the ITD. The cone is approximately 432 mm (17 in) long and 149.4 mm (5.88 in) wide and is attached to the 149 mm Teflon core that resides within the nacelle. The cone half angle was machined at 10 degrees. The combination of cone angle and ITD wall offset redirects the flow away from the simulator centerline (Figure 1) and increases the cross-sectional area by a factor of approximately three. This geometric change occurs abruptly at the interface between the air supply duct and ITD, and is therefore considered to be a sharp or discontinuous surface boundary.

After passing through the ITD, the flow is abruptly redirected inward by 10 degrees into a straight annular section. The redirection of flow is discontinuous on both the inner surface (simulating the scaled engine core) and outer duct surface (simulating the scaled engine nacelle). The straight annular section, referred to as the nacelle proper, has a constant spacing (H) of 74.7 mm (2.94 in) and extends downstream 1.22 m (48 in), or approximately 16 H.

After exiting the nacelle section, the flow enters the Exit Transition Duct (ETD) and is redirected inward 10 degrees toward the simulator centerline. At the entrance of the ETD, the inner core undergoes a sudden transition back to a conical surface with a sharp trailing edge, thereby producing a converging annular section.

At the exit of the ETD, a transition occurs through a surface discontinuity from a converging annulus channel to a straight exhaust tube. This 152.4 mm (6 in) diameter exhaust tube extends downstream approximately 40 diameters before undergoing a sudden enlargement where the exiting air expands into a PVC tube with an internal diameter of 30.5 cm (12 in) and is directed outside of the test chamber.

Inlet Flow Boundary Conditions

Flow conditions upstream of the quarter-scale engine nacelle were determined by matching the Reynolds number (based on the diameter in the annular region) between the full-scale and quarter-scale nacelle simulators, for a specified mass flow rate. Air at ambient temperature and pressure (T_{amb} and P_{amb}) was used to supply the flow facility in all tests. Supply air density was computed using the local temperature and pressure of the surrounding air. Typical values of P_{amb} = 98.7 kPa (14.37 psia) and T_{amb} = 293 K (73 °F) resulted in a computed density of 1.2 kg/m^3 (0.0748 lbm/ft^3). From this density, a mass flow rate of 0.344 kg/s (0.757 lbm/s) was determined for the quarter-scale nacelle. Assuming uniform flow, the average velocity within the 152.4 mm (6 in) air supply tube was 15.7 m/s (51.5 ft/s). Under these conditions the inlet flow Reynolds number based on tube diameter, Re_D was estimated to be 172,000.

Data Acquisition Strategy

Velocity traverses across the inlet air supply tube, as well as several locations throughout the expansion and contraction annular regions, were taken using Laser Doppler Anemometry (LDA) configured in backscatter mode. Velocity and turbulent intensity profiles were obtained at 11 measurement stations as determined from pre-test calculations. Table 1 provides a complete listing of the LDA measurement stations along with their relative streamwise location. Measurement locations, designated by MS-1 through MS-11, are also presented schematically in Figure 2. It is important to note that MS-1 and MS-2 are located upstream of the inlet cone and therefore these stations are listed as negative quantities.

Velocity data acquired at stations MS-1 and MS-2, in the air supply tube, document the conditions of the approach flow and MS-1 serves as the inflow boundary condition for the CFD calculations. Measurement station 1 was located 40.8D (6.2 m or 245 in) downstream from the flow conditioning section, and MS-2 was 44.8D downstream. The relative locations of stations 1 and 2 were therefore positioned upstream of the inlet transition duct (ITD) by –629 mm (-24.76 in) and -47 mm (-1.87 in), respectively.

To enable LDA measurements in the presence of the curved surfaces that comprise the simulator, flat removable windows were installed into machined openings at each measurement station. Windows were installed such that the intrusion into the flow field was minimal, resulting in a 1.6 mm reduction in the effective diameter at the measurement plane.

During each experiment, the blower speed was set to the desired mass flow rate and the local air speed within the supply tube was continually monitored using a pitot-static pressure probe connected to a differential magnetic pressure gage. For reference purposes, the probe was positioned within the air supply tube approximately 40 mm away from the tube wall and approximately 20D downstream of the flow conditioning section.

Velocity profile data were acquired using a Dantec 55X laser Doppler anemometry system (LDA) with illumination from an Argon-Ion laser operating at 488nm (blue component) and 514.5 nm (green component). The LDA system was configured in the backscatter mode, with a focal length of 310 mm (12.25 in), and was mounted on an optical bench with three degrees of freedom. Spatial positioning of the LDA measuring volume was obtained by manual adjustment of the bench using an xyz traverse with a range of approximately 305 mm (12 in) in each of the three directions. The spatial resolution in the x-y plane (a plane parallel to the nacelle centerline) was nominally +/-127 microns (0.005 in), and the vertical or z component was +/- 2.5 mm (0.1 in).

LDA measurements were performed in only one spatial direction. Given the optical configuration of the present LDA system, measurement volume dimensions of approximately 86 microns in diameter and 0.735 mm in length were estimated. Scattered signals from the photo detectors were frequency shifted by 40 MHz and passed to a counter type signal processor. Tests were conducted with the current LDA setup to determine the number of samples necessary to provide repeatable data. Higher data rates resulted from the selection of the green laser beam component at 514.5 nm. Sample sizes of 300, 400, and 500 were evaluated and found to differ by less than 6 cm/s. The present LDA acquisition system was therefore set to acquire 300 data points at each spatial location. To provide additional confidence in the LDA data, several velocity traverses were acquired at most measurement stations. Typically, each velocity traverse consisted of 45 spatial locations measured across the diametrical plane of the tube. In addition, at each measurement station, the LDA optics was reoriented such that the each traverse was always performed normal to the streamwise flow direction.

LDA measurements are based on the ability to adequately seed the flow field of interest with micron-sized particles. Seed material in the present study was generated by the vaporization of a solution mixture (75% propylene glycol and 25% water) using a commercial smoke generator. The fog was introduced at the blower inlet producing a well-mixed, densely seeded, flow at the blower exit with nominal particle sizes between 1 and 6 microns. Stokes number estimates ranged from 0.006 in the central region of the tube to 0.13 at the walls. Statistical uncertainty in the mean velocity measurements varied between +/-0.27 m/s in the nacelle region to +/-0.22 m/s in the core region.

Numerical Modeling

Post-test calculations of the flow in a quarter-scale nacelle have been obtained using both the VULCAN and CFD-ACE models. The CFD-ACE code is best suited for numerical simulation of flows in complex geometries. VULCAN includes submodels required to simulate flow and fire dynamics phenomena and therefore makes some approximations to represent complex geometries. Notable differences between VULCAN and CFD-ACE include the Cartesian grid as opposed to the body-fitted coordinate system in CFD-ACE and the ability to model fires with VULCAN, which is not possible with CFD-ACE. This section provides additional background information on each code.

VULCAN

VULCAN has been developed over the past 8 years at Sandia National Laboratories (SNL). VULCAN is derived from the KAMELEON fire model from the SINTEF Foundation and the Norweigian University of Science and Technology (NUST) [5,6] and uses an extension of the SIMPLEC method of Patankar and Spalding [7] to solve the conservation equations on a structured, staggered, three-dimensional Cartesian grid. The "brick" mesh is employed in part to facilitate rapid solutions of participating media radiative heat transfer. The ability to resolve the geometry of the system is only limited by the ability to construct the appropriate grid with the Cartesian grid generator available in VULCAN. A second-order accurate upwind scheme is used for the convective terms. Turbulence is modeled using a standard two equation k-ε model with wall functions. Combustion is based on Magnussen's Eddy Dissipation Concept [7] with infinitely fast combustion assumptions. Models of soot generation and oxidation are also included.

CFD-ACE

CFD-ACE is a pressure-based commercial code [8,9] that solves the Farve-averaged Navier-Stokes equations. The code uses a cell-centered control volume approach to discretizing the governing equations. It employs an iterative solution scheme in which the assembled equations for each dependent variable are solved sequentially and repeatedly to reduce errors to acceptably low values.

Various modeling options are available. In the present calculations, the governing equations were solved until a steady-state solution was reached. Heat transfer was not modeled. The code was applied using the incompressible option with a single fluid (air) and the k-ε turbulence model of Launder and Spalding [10] with wall functions. In addition, the k-ω turbulence model of Wilcox [11] and the Low Reynolds number k-ε turbulence model of Chien and Smith [12] were used in sensitivity calculations. First-order upwind spatial differencing was used for the turbulence quantities and 90% second-order upwind spatial differencing (with 10% first order blend) was used for the velocity and density. The structured grid utilized a body-fitted coordinate system with multiple domains.

Modeling Geometry

The geometry used in the fluid flow simulations was a quarter-scale version of a representative full-scale nacelle geometry, slightly revised for modeling purposes. To ensure consistency with the existing data [13], the full-scale nacelle geometry has the same basic dimensions as the nacelle simulator section used in the AENFTS for the Halon Alternatives program. Enhancements include the reduction of geometric complexity posed by view ports on the outer walls. The surface-of-revolution geometry considered in these analyses does not contain any internal clutter. Nomenclature for primary parts are the inlet pipe, outlet pipe, nacelle and core. Figure 2 provides the dimensions for the pipes, nacelle, and the core. The presence of wires or struts used to support the core was neglected in the simulations. All corners and tips have been considered sharp (i.e. - radius of zero). The windows in the nacelle wall were not modeled. It should be noted that the nacelle geometry was modeled starting at measurement station 1, where experimental data were acquired to use as exact input. None of the inlet flow conditioning screens, honeycombs (tubes), etc. were modeled. The modeled geometry ended 10 pipe diameters downstream of the core region, which is 6 pipe diameters downstream of the final measurement station (MS-11).

Grid Structure

VULCAN

VULCAN uses a Cartesian grid system that induces some inaccuracies in the representation of the geometry for the diverging and contracting regions of this configuration. The transition regions appear as "stairs" rather than straight, angled lines. A portion of the grid is shown in Figure 3. The grid was refined in selected areas, such as the transition regions, allowing the important flow characteristics to be determined. In areas where the geometry was straight, such as the inlet, exit, and annular regions, the computational cells were stretched.

The length of the geometry created a grid with many computational cells. The grid was generated using the VULCAN Graphical User Interface. The final Cartesian grid consisted of 196 (X-direction) by 45 (Y-direction) by 45 (Z-direction) grid points for a total of 396,900 cells in the simulation. The cells in the cross-section were 0.007 x 0.007 m^2, while the minimum cell length in the axial direction was 0.0085 m and varied along the pipe (refined in transition regions and stretched in the exit pipe and other straight sections). The simulation time was approximately 5 days on an UltraSPARC 250 MHz processor. The solution was converged such that all residuals were reduced 5 orders of magnitude.

CFD-ACE

The computational grid used in CFD-ACE calculation was generated with the commercial code Gridgen [14]. A three-dimensional (3-D) grid was used in the simulation, instead of an axisymmetric grid, in order to capture any potential swirling flow, which may have resulted due to flow conditioners, and also to allow for future 3-D geometric features. The structured, three-dimensional (3-D), multi-block grid consisted of 301 axial (primary flow direction) points, 25 radial points, and 48 circumferential points, for a total of 361,200 grid points. Example slices from the grid are shown in Figure 4. Axial grid spacing in the annular (nacelle/core) region varied from 0.006 m (0.25 in) near the corners of expansion/contraction to 0.018 m (0.69 in) in the middle section of constant diameter flow. Radial spacing was approximately 0.002 m (0.08 in) throughout the annulus. Circumferential spacing was constant at 7.5 degree increments which relates to linear (arc) dimensions of 0.020 m (0.77 in) at the maximum nacelle diameter to 0.010 m (0.39 in) at the maximum core diameter. In addition to the 'fine' three-dimensional (3-D) grid solution, a coarser mesh solution (ACE-Coarse) was obtained. The coarse mesh was generated by extracting every other grid point in all three directions from the fine mesh. The coarse mesh contained 151 axial points, 13 radial points, and 24 circumferential points, for a total of 47,112 grid points. In both mesh simulations, convergence was obtained such that all residuals of interest (velocity, pressure, turbulence) were reduced more than 5 orders of magnitude. The fine mesh solution required 400 Mbytes of memory, 2200 iterations and 15 days computing time on a Sun Microsystems UltraSPARC 250 MHz processor, while the coarse mesh solution required less than 1 day of computing time.

Boundary Conditions

The boundary conditions used in the 3-D turbulent CFD simulations were applied to best represent the experimental conditions. In some cases, a slight deviation from the experimental conditions was necessary. The boundary conditions will be fully discussed in this section.

Inlet Velocity

The experimental data measured at the inlet (MS-1) showed a slight asymmetry in the velocity profile. It was not possible to specify this asymmetric velocity profile as an inlet boundary condition in the calculations since only a radial profile was required. Instead, a symmetrical profile (log-law relationship: $u/u_{\max} = (y/R)^{0.12}$) was used and the agreement with the measured inlet profile is shown in Figure 5. In both cases, the maximum velocity is 20.07 m/s.

Inlet Turbulence Intensity

Similar to the inlet velocity, the inlet turbulence intensity data was also asymmetric. The boundary condition for the calculations used a symmetric inlet turbulent intensity based on a parabolic curve fit of experimental data. This was accomplished by splitting the experimental data set at the midpoint, mirroring both sides across the centerline, and fitting a parabolic curve to the resulting data set (see Figure 6). The resulting equation for the inlet turbulence intensity is shown on the plot.

Turbulence intensity is not a direct variable used in the codes and approximations must be introduced in order to relate the experimental definition of the turbulence intensity to that employed in the codes. In the experiment, turbulence intensity, I, is determined from the measurements using the following equation:

$$I = \frac{\sqrt{\overline{u_s'^2}}}{\overline{u_s}}$$

The bar symbol represents the mean of the squared value, u_s' is the fluctuating streamwise velocity, and $\overline{u_s}$ is the mean flow streamwise velocity. In the k-ε turbulence model, the definition of the turbulent kinetic energy is:

$$k = \frac{\overline{u'^2} + \overline{v'^2} + \overline{w'^2}}{2} = \frac{\overline{u_s'^2} + \overline{v_c'^2} + \overline{w'^2}}{2}$$

Assuming isotropic turbulent flow, i.e., $u_c' = w' = u_s'$, and using the experimental definition of turbulence intensity, the turbulent kinetic energy becomes:

$$k = \frac{3\overline{u_s'^2}}{2} = \frac{3(I\overline{u_s})^2}{2}$$

The above equation was used to define the turbulent kinetic energy at the inlet plane and to determine the turbulence intensity from the turbulent kinetic energy predicted at each measurement station.

Outlet Boundary Condition

At the outlet of the nacelle geometry, a constant pressure condition was specified using ambient conditions of 98.7 kPa and 293 K. The outlet was located 10 pipe diameters downstream of the nacelle/core region, which was 6 pipe diameters downstream of the final measurement plane (MS-11).

Wall Conditions

Along each surface of the nacelle geometry, a no-slip wall was specified at a constant temperature of 293 K. Surface roughness was not included in either simulation. In addition, wall functions were used to represent the flow next to the wall when the k-ε turbulence model was employed; otherwise, the solution was directly integrated to the wall when either the k-ω turbulence model or the Low Reynolds number k-ε turbulence model were employed.

Results

VULCAN and CFD-ACE calculations of air flow in a smooth nacelle geometry were performed. The streamwise velocity component and turbulence intensity values were measured in the experiment conducted at 46 Test Wing at Wright-Patterson Air Force Base [14]. A comparison of the numerical predictions and the experimental data at eleven measurement stations was performed. Selected measurement stations are shown in this paper. As discussed previously, the inlet velocity and turbulence intensity values at measurement location 1 were specified to be the curve fit values of the experimental data. The exact measurement locations and geometric reference locations are shown in Table 1. The results shown below are for a vertical slice through the geometric centerline at each location. The VULCAN results are based on values at cell centers while the CFD-ACE results are based on values at the grid points.

Measurement Plane 3

Figures 7 and 8 show the velocity and turbulence intensity profiles predicted by VULCAN and CFD-ACE at the first measurement plane in the transition region of the core. In the core region, the position ranges from 0.0 at the nacelle wall to 76.2 mm at the core wall. As shown in Figure 7, both sets of velocity predictions agree well with experimental data. Although the VULCAN prediction and the data appear to be in closer agreement near the walls, VULCAN does not have adequate resolution in the wall regions due to the Cartesian grid structure and therefore this agreement is fortuitous. The data also show a dip in velocity and then a slight increase near the core wall. This feature may possibly be due to a slight misalignment between the core and the flow direction. A slight misalignment would cause the flow on the leeward side of the core to separate. In addition, it should be noted that the VULCAN velocity profile in this figure does not go to zero because the end point values displayed are not exactly at the wall. In Figure 8, both code predictions compare well overall with the turbulence intensity data. The CFD-ACE predictions deviate from the data and the VULCAN result by ~10% near both the nacelle wall and the core wall. This difference is to be expected, given that turbulence intensity is normalized by the mean flow velocity and the CFD-ACE prediction shows higher velocities next to the walls (in Figure 7). Figure 9 shows a plot of the root mean square (rms) of the fluctuating streamwise velocity (u_s') or the numerator of turbulence intensity. For this quantity, the CFD-ACE prediction shows much better agreement with the experimental data. Statistical uncertainty velocity values are estimated +/-0.20 m/s.

Measurement Plane 5

Figures 10 and 11 show the velocity and turbulence intensity profiles predicted by VULCAN and CFD-ACE at the third measurement plane in the transition region of the core. At this location, the velocity results are similar in the center of the channel and deviate from each other near the walls. In Figure 11, CFD-ACE predicts very large turbulence intensity values near the nacelle wall with decreasing levels across the channel to the core wall. VULCAN predictions show large turbulence values near the nacelle wall, decreasing levels across the channel, and then a sudden increase in turbulence intensities near the core wall. This increase near the core wall could be attributed to the stair-stepped grid along the wall, which tends to reduce the streamwise flow and increase the cross-stream flow, thereby, causing higher turbulence levels. The experimental data show slightly higher values near the nacelle wall with decreasing values towards the core wall where some noise in the data is evident. The measurement uncertainty associated with the noise in the data near the wall is difficult to quantify. Again, these large differences between the CFD predictions and the experimental data near the nacelle wall can also be attributed in part to the differences in mean velocity. When the rms values of u_s' are plotted in Figure 12, both code predictions are in much better agreement with the experimental data. Statistical uncertainty in the measured mean velocity was estimated at +/-0.20 m/s.

Measurement Plane 7

Figures 13 and 14 show the velocity and turbulence intensity profiles predicted by VULCAN and CFD-ACE at the second measurement plane (or mid-plane) in the straight section of the core. At this location, the velocity predictions shown in Figure 13 are in very good agreement with the experimental data. At this location, any misalignment between the core and the flow direction would be minimized. In Figure 14, both code predictions of turbulence intensities show reasonable agreement with the data. Near the walls, the data show both larger turbulence intensity values and higher levels of noise. It should be noted that the experimental data at this measurement station (and at MS-9) does not span the entire distance to the core wall. Statistical uncertainty in the measured mean velocity was estimated at +/-0.22 m/s.

Measurement Plane 9

Figures 15 and 16 show the velocity and turbulence intensity profiles predicted by VULCAN and CFD-ACE at a measurement plane centered in the rear transition region of the core. The CFD-ACE velocity predictions shown in Figure 15 are in very good agreement with the experimental data; whereas, the VULCAN predictions show the velocity decreasing near both walls and increasing in the center of the channel. This feature is due to the stair-stepped grid along the angled walls, which tends to direct the flow into center of the channel. In Figure 16, both CFD-ACE and VULCAN predict approximately 10% lower turbulence intensity values than the experimental data. At this location, two different experimental data sets (DATA and DATA2) were included so that an assessment of the repeatability of the tests can be made. Notice that DATA2 does not include the region near the nacelle wall where increased noise levels in the data exist. Statistical uncertainty in the measured mean velocity was estimated at +/-0.20 m/s.

Measurement Plane 11

Figures 17 and 18 show the velocity and turbulence intensity profiles predicted by VULCAN and CFD-

ACE at the final measurement plane in the outlet section. In Figure 17, the predicted velocity profiles show the wake diminishing with increasing distance from the core. The experimental data do not illustrate the presence of a wake region and in addition, appear to contain increased noise levels. There are noticeably fewer data points across the diameter of the pipe. The turbulence intensity values measured in the experiment are considerably higher than the CFD predictions as shown in Figure 18. In addition, the experimental values have increased by a factor of three from the previous measurement location (MS-10). CFD-ACE predicts constant turbulence intensity values below 10% for the majority of the flow across the pipe.

Sensitivity Study

Two different sets of simulations using CFD-ACE were performed to assess the sensitivity of the results to the grid size and the turbulence models. In the first simulation, the coarsened computational grid, with 47,112 grid points, was used with the standard k-ε turbulence model. The ACE-COARSE prediction was compared to the original CFD-ACE solution and the experimental data at measurement location 3. In the second set of simulations, two calculations were performed, one with the k-ω (ACE-KOMEGA) turbulence model and the other with the Low Reynolds Number k-ε (ACE-LRE) turbulence model, to investigate the effect of wall functions on the solution. In order to reduce computational time, a 2-D axisymmetric calculation was performed and compared to the 3-D solution and the results were identical. Therefore, the k-ω and low Reynolds number calculations were performed using a 2-D fine mesh. Both turbulence model results were compared to the original CFD-ACE solution and the experimental data at measurement location 3.

Coarse Grid Results

Figures 19 and 20 show the predicted velocity and turbulence intensity profiles for the ACE-Coarse solution at the first measurement plane (MS-3) in the transition region of the core. In both figures, the ACE-Coarse solution matches the CFD-ACE solution, except in the near wall regions. This difference results from the lack of grid resolution near the nacelle and core walls in the coarse grid solution. Similarly, the coarse mesh solution (ACE-Coarse) showed good agreement with the fine mesh solution (CFD-ACE) at the other measurement locations, with only minor differences near walls.

k-ω and Low Reynolds Number Turbulence Model Results

At measurement location 3 (Figure 7), large differences in velocity results occurred between the CFD-ACE solution and the experimental data near the core wall. A numerical study was performed to determine if the wall functions used in the CFD-ACE solution failed to capture the velocity dip near the core wall. It is well known that wall functions fail in regions where large adverse pressure gradients exist and for this case, the majority of the inlet transition duct did contain an adverse pressure gradient. For both turbulence model cases, a 2-D axisymmetric calculation was performed using the same number of grid points (301) as the fine mesh in the axial direction. In the radial direction, the number of grid points was increased from 25 to 150 so that a nominal y^+ value of 0.3 was achieved at the first grid point away from both the nacelle wall and the core wall.

Figures 21 and 22 show the predicted velocity and turbulence intensity profiles for both the ACE-KOMEGA and ACE-LRE solutions at the first measurement plane in the transition region of the core. The ACE-KOMEGA velocity profile, shown in Figure 21, is very similar to the ACE-LRE solution. In addition, these solutions are consistent with the CFD-ACE solution in that they do not predict a velocity dip near the core wall. As expected, slight differences did occur near both walls due to the use of wall functions in the CFD-ACE solution. In Figure 22, the turbulent intensity values for the ACE-KOMEGA solution and the ACE-LRE solution differ slightly near the walls. In addition, both solutions predict lower turbulence intensity values than the experimental data near the core wall. A better comparison can be made by plotting the rms value of u_s', as shown in Figure 23. In this figure, both the ACE-KOMEGA solution and the ACE-LRE solution show slightly better agreement with the experimental data, except near the core wall where all CFD predictions still differ from the data.

Overall, the use of wall functions did not severely impact the solution for this type of application. For this reason, it is even more likely that a small misalignment between the core and the flow direction caused the velocity dip near the core wall at measurement location 3.

Summary

Numerical simulations of air flow through a quarter-scale smooth nacelle geometry were performed using the VULCAN code and the CFD-ACE code. Comparisons of the numerical predictions with the experimental data from the 46 TW Aerospace

Survivability and Safety Flight at WPAFB were performed in order to benchmark the CFD codes for this application. In general, the velocity predictions showed good agreement with the data in the center of the channel throughout the entire geometry but deviated near the walls. The turbulence intensity predictions also showed good agreement along the inlet section and at the start of the inlet transition duct section. The numerical predictions showed much larger turbulence intensity values in most of the inlet transition duct section and at the start of the straight annular section. These differences between the predictions and the experimental data were significantly affected by to differences in mean velocity values, since mean velocity was used to normalize the turbulence intensity. When the rms values of the fluctuating streamwise velocity were plotted, the CFD predictions showed much better agreement with the experimental data. At the remaining downstream measurement planes, the data consistently showed larger turbulence intensity values, although the trends were similar. Some differences were observed between VULCAN and CFD-ACE results due to the Cartesian grid structure used by the VULCAN code. These differences mainly occurred in the inlet transition duct and the outlet transition duct where the walls are angled. Also, the experimental data tended to show poorer resolution near the walls of the transition ducts. This occurrence may be due to the low signal to noise ratio as affected by wall curvature. In addition, it is also possible that a small misalignment between the core and the flow direction occurred in the experiment. A misalignment could explain some of the differences between the CFD predictions and the experimental data, especially in the inlet transition duct section.

In addition to the above comparisons, sensitivity studies were also performed using CFD-ACE in order to assess the effect of grid resolution and turbulence models on the results. First, a calculation was performed using a coarse mesh (factor of 7.7 less grid points). Overall, the coarse mesh solution showed good agreement with the fine mesh solution; differences were only observed near the walls due to the lack of grid resolution. In addition, a second set of simulations using both a k-ω model and a Low Reynolds Number k-ε model were performed to assess the effect of using wall functions. Small differences did result near the walls but the use of wall functions did not severely impact the numerical predictions for this application. Overall, this effort provided a benchmark case for both the VULCAN and CFD-ACE codes for the application of interest.

Acknowledgments

The authors would like to thank Dave Keyser (Naval Air Systems Command) for coordinating this activity and for his insight into the DoD applications. Also, the authors wish to express their appreciation to Paul DesJardin (Sandia National Laboratories) and Vernon Nicolette (Sandia National Laboratories) for their consultation on the numerical modeling and Walter Gutierrez (Sandia National Laboratories) for his previous efforts on modeling this problem. Finally, the authors would like to thank Lawrence Ash (NAVAIR) for initiating and organizing the project.

This work is part of the Department of Defense's Next Generation Fire Suppression Technology Program, funded by the DoD Strategic Environmental Research and Development Program. Additional funding was provided by the USAF 46 Test Wing Aerospace Survivability and Safety Flight at Wright-Patterson Air Force Base, Ohio.

References

1. Hamins, A., Cleary, T., Borthwick, P., Gorchkov, N., Mcgrattan, K., Forney, G., Grosshandler, W.L., Presser, C., and Melton, L., "Suppression in Engine Nacelle Fires, Section 9.4, Flow Field Modeling and Validation in a Mock Nacelle" in Fire Suppression System Performance of Alternative Agents in Aircraft Engine and Dry Bay Laboratory Simulations, NIST SP890, R.G. Gann, ed., pp. 84-104, 1995.

2. Wright Laboratory Technical Report WL-95-3077. Wright-Patterson AFB, Dayton, Ohio, 1995.

3. Wright Laboratory Technical Report WL-97-3076. Wright-Patterson AFB, Dayton, Ohio, 1997.

4. Lopez, A.R., Gritzo, L.A., and Hassan, B., "Computational Fluid Dynamics Simulation of the Air/Suppressant Flow in an Uncluttered F18 Engine Nacelle." Proceedings of the Halon Options Technical Working Conference, New Mexico Engineering Research Institute, Albuquerque, NM, pp. 281-297, 1997.

5. Holen, J., Brostrom, M., and Magnussen, B.F., "Finite Difference Calculation of Pool Fires." *The Twenty-Third Symposium (International) on Combustion*, The Combustion Institute, Pittsburgh, p. 1677-1683, 1990.

6. Magnussen, B.F., Hjertager, B.H., Olsen, J.G., and Bhaduri, D., "Effects of Turbulent Structure and Local Concentrations on Soot Formation and Combustion in C2H2 Diffusion Flames." *The Seventeenth Symposium (International) on Combustion*, The Combustion Institute, Pittsburgh, p. 1383-1393, 1979.

7. Patankar, S.V., and Spalding, D.B., *Int. J. Heat Mass Transfer*, 15:1787, 1972.

8. CFD-GUI™, CFD-ACE Structured Flow Solver Manual, Version 5, CFD Research Corporation, Huntsville, Alabama, October, 1998.

9. CFD-ACE™, Theory Manual, Version 5, CFD Research Corporation, Huntsville, Alabama, October, 1998.

10. Launder, B. E. and Spalding, D. B., "The Numerical Calculation of Turbulent Flows", *Computational Methods Applied to Mechanics and Engineering*, 3, pp. 269-289, 1974.

11. Wilcox, D.C., "A Half Century Historical Review of the k-ε model," AIAA-91-0615, 1991.

12. Chien, T. and Smith, A.M.O., *Analysis of Turbulent Boundary Layers, Academic Press*, New York, 1982.

13. Bennett, J.M., Caggianelli, G.M., Kolleck, M.L., and Wheeler, J.A., "HALON REPLACEMENT PROGRAM FOR AVIATION Aircraft Engine Nacelle Application Phase I – Operational Parameters Study," WL-TR-95-3077, 1997.

14. Gridgen User Manual, Version 13, Pointwise, Inc., Bedford, Texas, 1998.

15. Disimile, P. and Tucker, J., Personnel communication on the experimental results for tests conducted at Wright Patterson Air Force Base, 2001.

Tables

Reference	Cone LE downstream from flow conditioner exit	-6832.6	-269
MS-1	Upstream from Cone LE	-619.125	-24.375
MS-2	-47mm (-1.875") Upstream from Cone LE	-47.625	-1.875
Reference	Start of ITD	-1.016	-0.04
Reference	Start Cone/Engine Core LE	0	0
MS-3	Downstream from Cone LE and within the ITD	60.325	2.375
MS-4	Downstream from Cone LE and within the ITD	196.85	7.75
MS-5	Downstream from Cone LE and within the ITD	314.325	12.375
Reference	Nacelle Proper/ITD surface discontinuity (End ITD)	415.036	16.34
Reference	Cone TE	428.752	16.88
MS-6	Downstream of ITD/Nacelle surface discontinuity	457.962	18.03
MS-7	Downstream of ITD/Nacelle surface discontinuity	1028.7	40.5
MS-8	Downstream of ITD/Nacelle surface discontinuity	1596.136	62.84
Reference	Nacelle Proper/ETD surface discontinuity (Start ETD)	1634.236	64.34
Reference	Start Cone/Engine Core LE	1634.236	64.34
MS-9	Downstream from Nacelle/ETD surface discontinuity	1831.086	72.09
Reference	End of ETD	2050.288	80.72
Reference	Cone/Engine core Trailing edge (TE)	2066.036	81.34
MS-10	Downstream from Cone TE	2116.836	83.34
MS-11	Downstream from Cone TE	2675.636	105.34
Reference	Sudden expansion from 6" to 12" PVC exhaust duct	8771.636	345.34

Note:
LE - Leading Edge
TE - Trailing Edge
ITD - Inlet Transition Duct
ETD - Exit Transition Duct

Table 1 - Locations of Measurement Stations

Figures

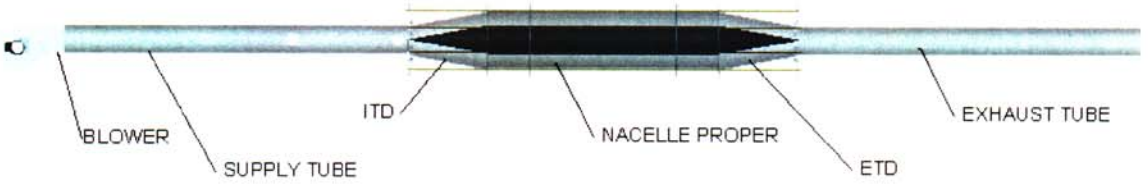

Figure 1 - Quarter-scale engine nacelle flow facility

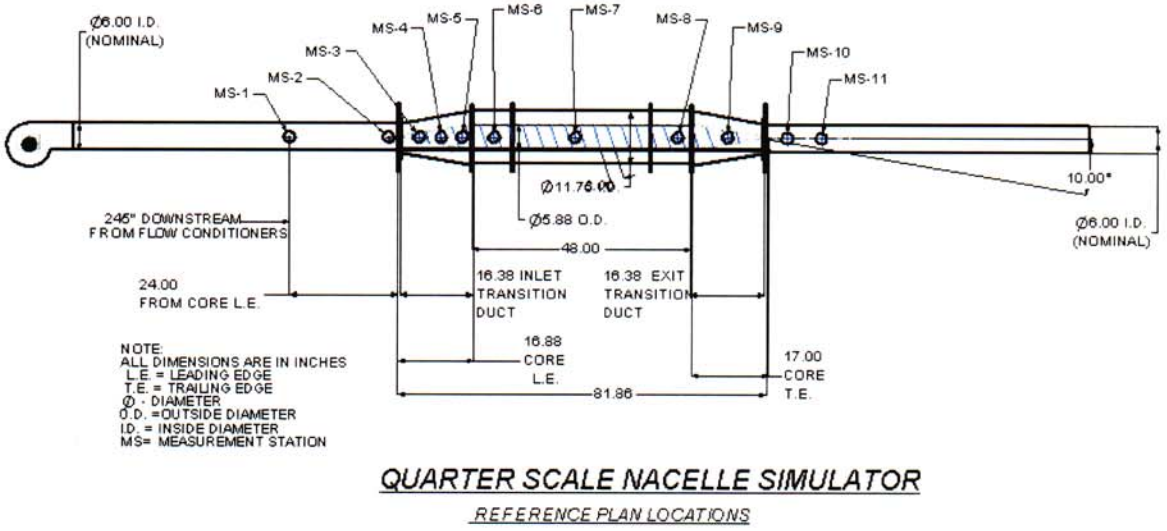

Figure 2 – Schematic of flow facility and measurement station locations

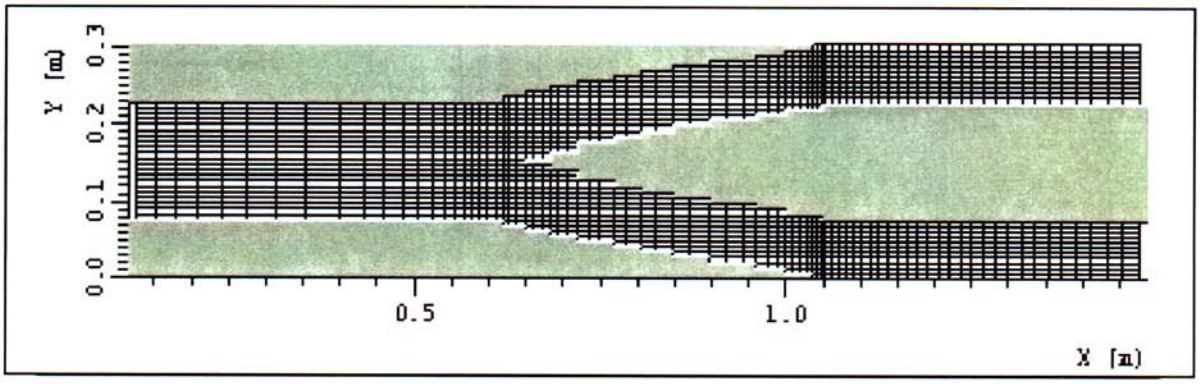

Figure 3 - Section of the VULCAN Grid Used in the Simulation

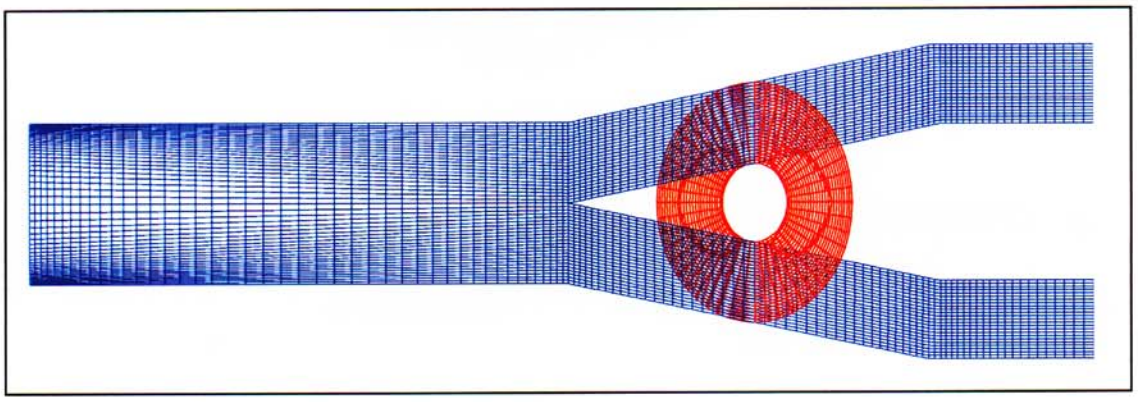

Figure 4 - Section of the CFD-ACE Grid Used in the Simulation

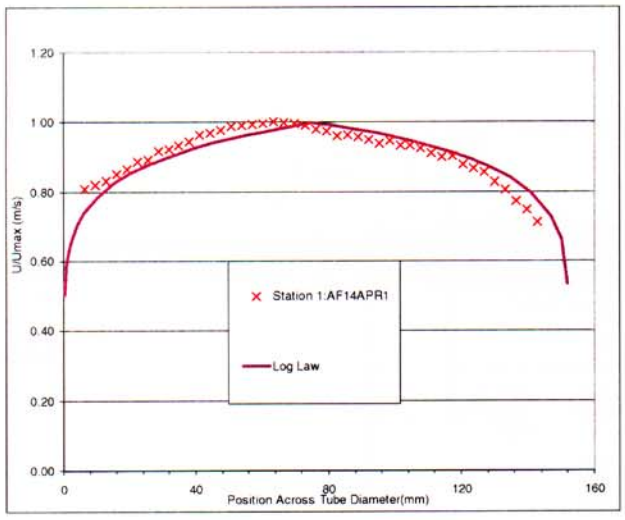

Figure 5 - Inlet Velocity Profile Comparison

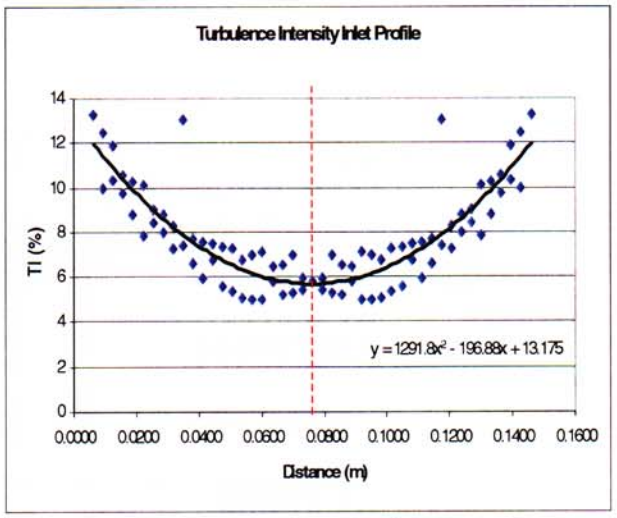

Figure 6 - Fit of Inlet Turbulence Intensity

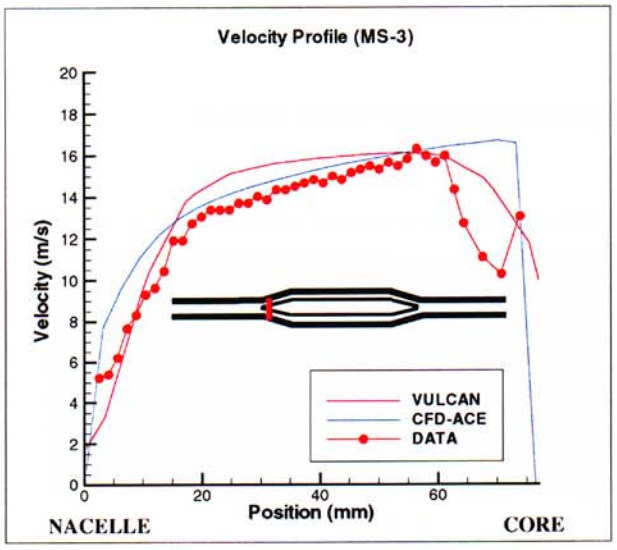

Figure 7 - Measurement Plane 3 Velocity Comparison

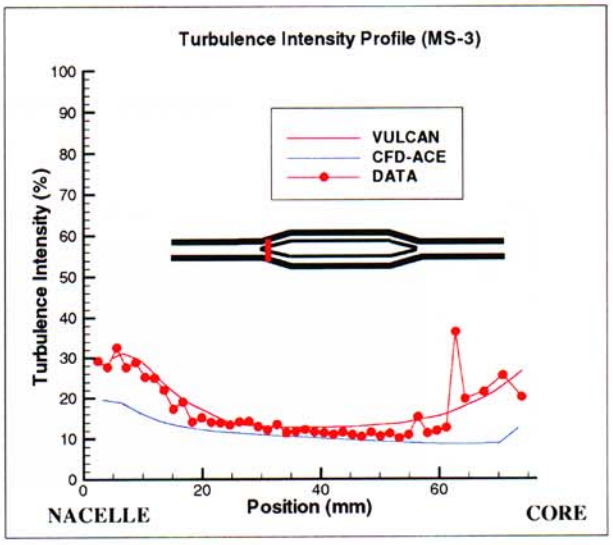

Figure 8 - Measurement Plane 3 Turbulence Intensity Comparison

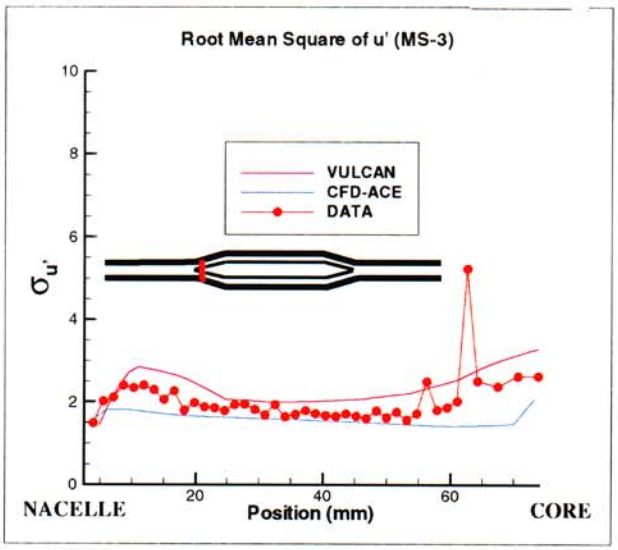

Figure 9 - Measurement Plane 3 Root Mean Square of u_s' Comparison

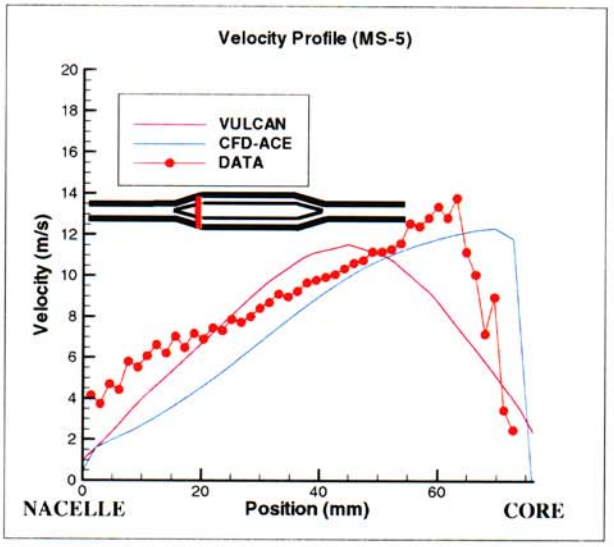

Figure 10 - Measurement Plane 5 Velocity Comparison

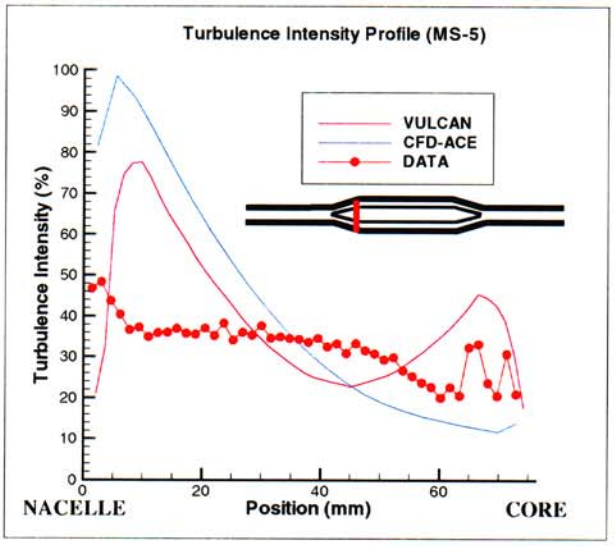

Figure 11 - Measurement Plane 5 Turbulence Intensity Comparison

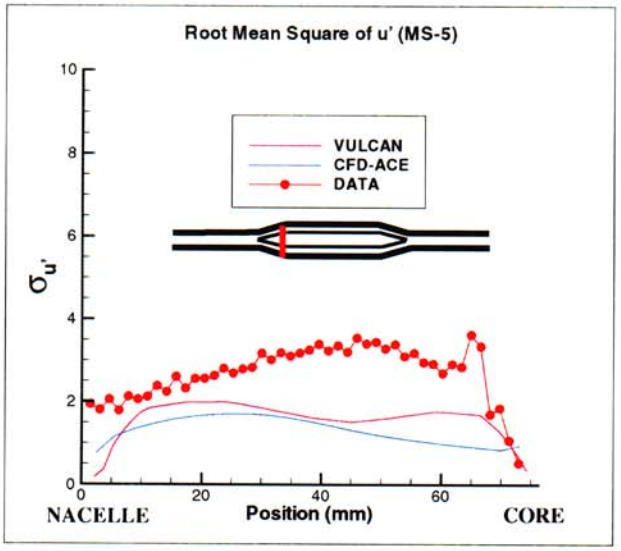

Figure 12 - Measurement Plane 5 Root Mean Square of u_s' Comparison

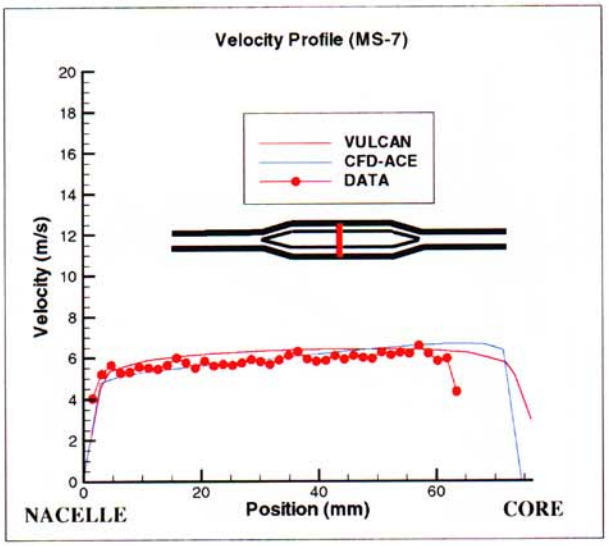

Figure 13 - Measurement Plane 7 Velocity Comparison

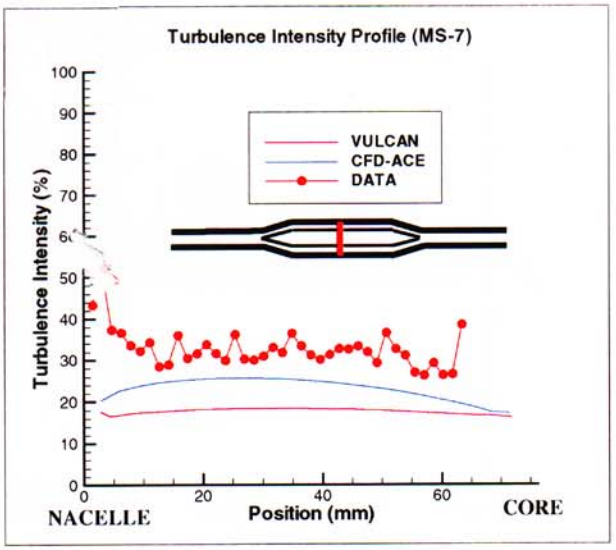

Figure 14 - Measurement Plane 7 Turbulence Intensity Comparison

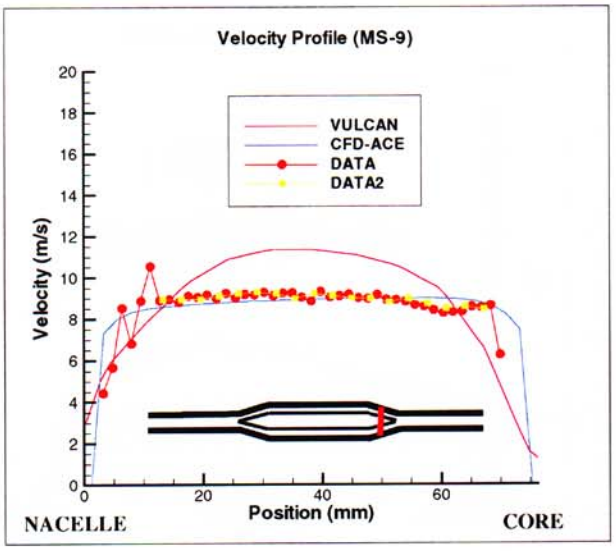

Figure 15- Measurement Plane 9 Velocity Comparison

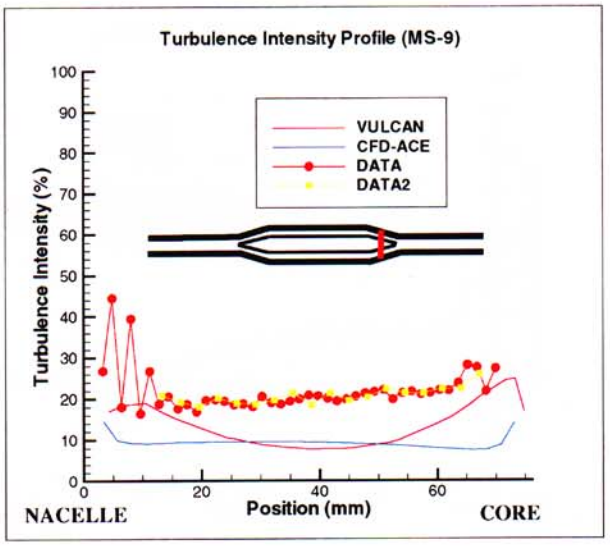

Figure 16 - Measurement Plane 9 Turbulence Intensity Comparison

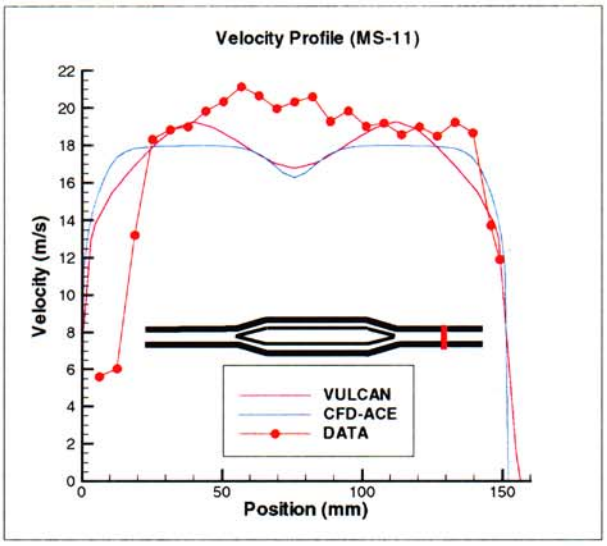

Figure 17 - Measurement Plane 11 Velocity Comparison

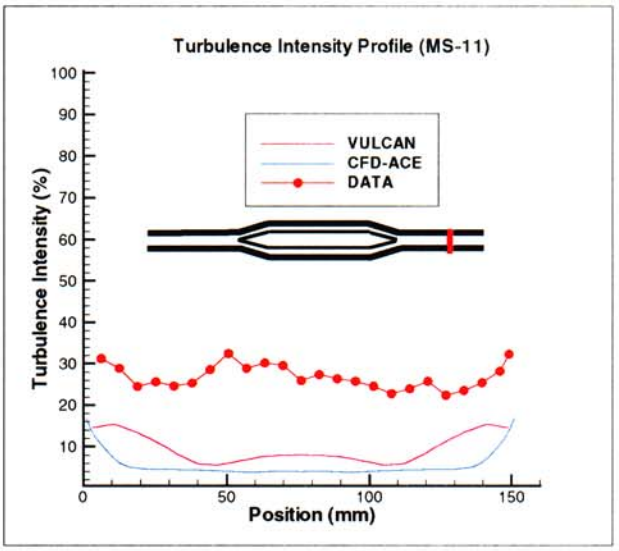

Figure 18 - Measurement Plane 11 Turbulence Intensity Comparison

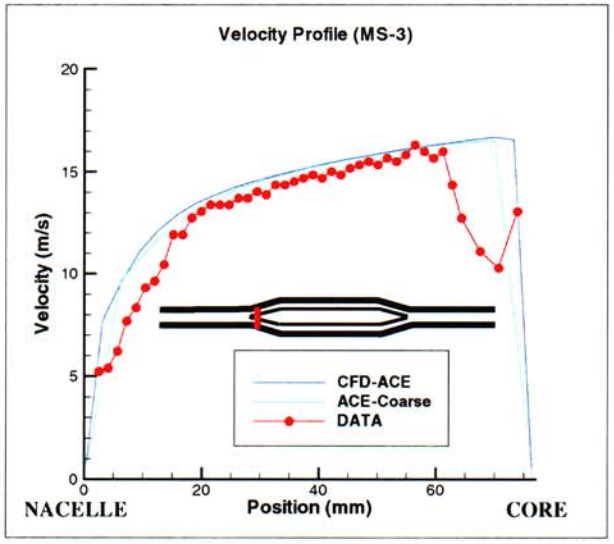

Figure 19 - Grid Sensitivity: Measurement Plane 3 Velocity Comparison

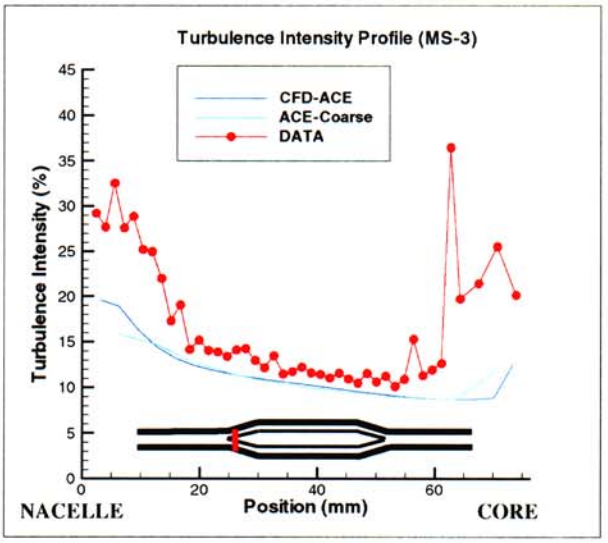

Figure 20 - Grid Sensitivity: Measurement Plane 3 Turbulence Intensity Comparison

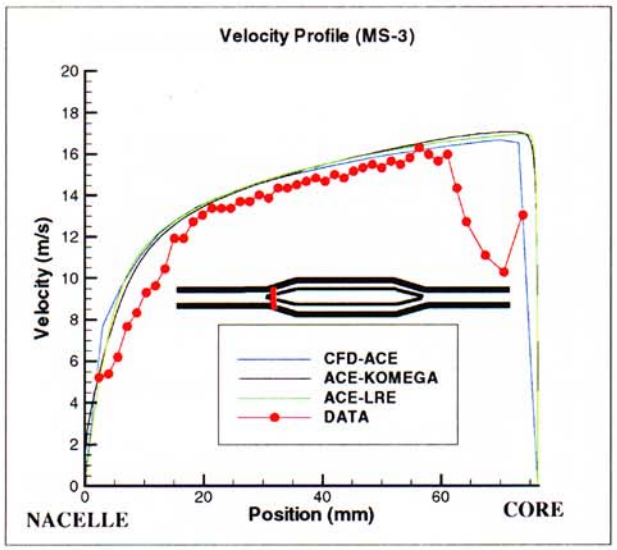

Figure 21 - k-ω and Low Reynolds Number Results: Measurement Plane 3 Velocity Comparison

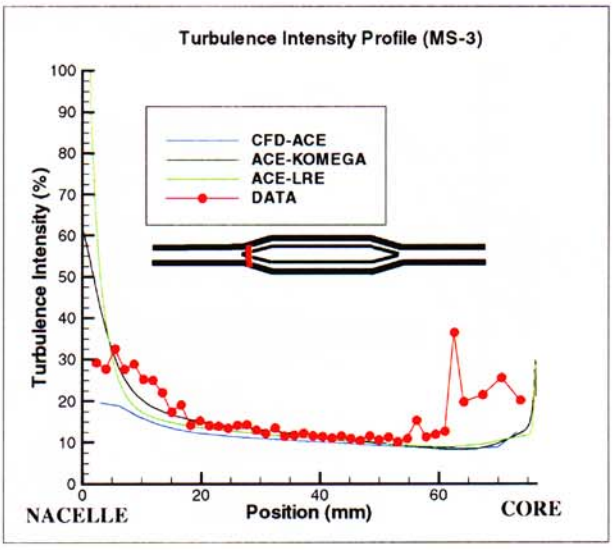

Figure 22 - k-ω and Low Reynolds Number Results: Measurement Plane 3 Turbulence Intensity Comparison

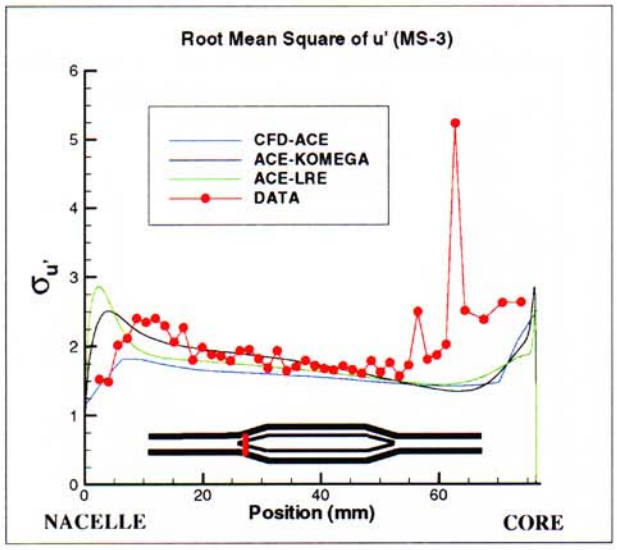

Figure 23 - k-ω and Low Reynolds Number Results: Measurement Plane 3 Root Mean Square of u_s' Comparison